Journal of Molecular Liquids 414 (2024) 126089

Contents lists available at ScienceDirect

Journal of Molecular Liquids

journal homepage: www.elsevier.com/locate/molliq

Thermodynamics, phase diagram, structure and anomalies of supercooled aqueous solutions of trehalose: A molecular dynamics study

Leonardo Perin, Paola Gallo *

Dipartimento di Fisica, Università Roma Tre, Via della Vasca Navale 84, I-00146 Roma, Italy

ARTICLE INFO

Keywords:
Supercooled water
Trehalose
Liquid-liquid critical point
Water anomalies

ABSTRACT

We perform molecular dynamics simulations of supercooled solutions of trehalose in TIP4P/2005 water, with concentrations of 20 and 40 wt% (weight percentage) in trehalose, a disaccharide often used in cryopreserving solutions. We analyze the thermodynamics and the structure of these solutions. From the isochores we find that in the 20 wt% solution the temperature of maximum density (TMD) line is still present and it is shifted to lower temperatures with respect to that of pure water. We also find that the Widom line and the liquid-liquid critical point (LLCP) are still present for this concentration and we estimate the position of the LLCP to be shifted at lower temperatures and slightly lower pressures with respect to that of pure water. In the 40 wt% solution we find that the TMD line still persists, but the region of density anomaly shrinks. No LLCP is observed down to the lowest temperature investigated, and maxima of the isothermal compressibility, used as proxy for the Widom line, become weaker. The water oxygen - water oxygen radial distribution functions keep on showing the typical distinction between high density and low density liquid found in pure water, but at low temperatures the presence of trehalose appears to favor the high density phase of water more than in pure water. The number of water molecules of the solvation shell confirms this picture.

1. Introduction

Trehalose aqueous solutions are relevant in many technological applications, such as the cryopreservation of biological molecules. In fact, it has been shown that this disaccharide possesses a remarkable ability to preserve biomolecules against freezing [1–13]. To investigate the role of trehalose in biological aqueous solutions, numerous experimental and computational studies have been carried out. Trehalose has been shown to affect both structural and dynamical properties of water by affecting the hydrogen bond network and by greatly slowing down the water relaxation processes upon cooling [13–22].

Monosaccharides and disaccharides are generally effective in cryopreservation. Trehalose was proven to be especially effective in several related properties, for example stabilizing living cells subjected to freezing stress [23,24] and slowing down more consistently hydration water dynamics [16]. Besides it shows better vitrification properties than other saccharides in water solutions [25].

In this context it is important to understand to what extent pure water characteristics in thermodynamics and structure are affected by the presence of trehalose.

As it is widely known, water displays many anomalous properties, some of the most renowned being the presence of a temperature of maximum density, that occurs at T = 277 K at ambient pressure, and the increase of the thermodynamics response functions in the supercooled region, the metastable state where water remains liquid below its freezing temperature [26–39].

The explanation for the water anomalies that has the largest consensus is the existence of a second-order phase transition point in the deeply supercooled region, the Liquid-Liquid Critical Point (LLCP), below which water would exist in two separate phases with different local structures, the high-density liquid (HDL) phase and the low-density liquid (LDL) phase, that are respectively linked to the two phases of glassy water, the high-density amorphous (HDA) and the low-density amorphous (LDA), observed experimentally [40–42]. The coexistence line between the two amorphous phases would be connected to that of the two liquid phases which ends at the critical point. This hypothesis was formulated by Poole, Sciortino, Essmann and Stanley [43] on the basis of molecular dynamics simulations with the ST2 potential model for water.

Experimental studies on supercooled water and water solutions have provided evidence of the presence of a liquid-liquid transition [44–48]

* Corresponding author.
E-mail address: paola.gallo@uniroma3.it (P. Gallo).

https://doi.org/10.1016/j.molliq.2024.126089
Received 26 June 2024; Received in revised form 29 August 2024; Accepted 19 September 2024
Available online 2 October 2024

and of the presence of maxima of the thermodynamic response functions (like the isothermal compressibility) [38] These maxima are connected to the presence of a line of maxima of the correlation length, the Widom line, that is always present in the one-phase region upon approaching a second-order critical point [49–52].

Computational studies play a central role in this field because with simulations it is possible to avoid the problem of crystallization, which is a major issue in experiments. Various water model potentials have been successfully employed for the study of the liquid and supercooled water, see for example SPC/E [53], MB-pol [54–56], WAIL [57]. The LLCP has been rigorously proven to exist for the water models ST2, TIP4P/2005, TIP4P/Ice, JAGLA and WAIL [58–64]. We note that the TIP4P/2005 and TIP4P/Ice are among the most accurate water models to investigate its thermodynamics and anomalies [65,66]. For TIP4P/2005 see for example Ref. 67–69 for the prediction of density maxima, density minima, isothermal compressibility and heat capacity minima and maxima, thermal expansion coefficient and shear viscosity, in agreement with experiments.

Recent research has been focusing extensively on aqueous solutions due to their widespread presence and to the fact that water is often more easily supercooled in solutions [26]. Many computational studies have shown the presence of a LLCP in several aqueous solutions of electrolytes, methanol, and perchlorates and hydrophobic solutes [70–75]. And recently a reversible liquid-liquid transition has been experimentally observed in a supercooled trehalose aqueous solution [48].

To better understand the effect of trehalose on the properties of water in this work we study through molecular dynamics (MD) simulations two solutions of TIP4P/2005 water and trehalose in the supercooled region, with concentrations of 20 wt% (weight percentage) and 40 wt% in trehalose. We analyze the thermodynamic and structural behavior of these solutions compared to pure water to study the effect of the solute on the anomalous properties of water.

The paper is organized as follows. In Section 2 details on the simulations are given, in Section 3 the thermodynamic results of the two solutions are analyzed, in Section 4 the structural results are reported, and in Section 5 conclusions are drawn.

2. Simulation details

MD simulations of binary mixtures of water and trehalose have been performed on two systems with different concentrations of the disaccharide: the first system is composed of 1500 water molecules and 20 trehalose molecules, corresponding to a concentration of 20.21 wt% in trehalose, and the second system is composed of 1498 water molecules and 54 trehalose molecules, corresponding to a concentration of 40.65 wt% in trehalose.

In Fig. 1 we show a representation of the trehalose molecule. A snapshot of the 20 wt% solution is reported in Fig. 2,

The MD simulations were carried out using the GROMACS 5.1.4 package [76]. The CHARMM force field was used for modeling the bonded and non-bonded interactions for the sugar [77,78], and the TIP4P/2005 potential was used for water molecules [65]. TIP4P/2005 is a well-known classical potential that is able to reproduce the behavior of the condensed phases of water [66]. The choice of this particular potential for our simulations is due to the fact that TIP4P/2005 is one of the best potentials to reproduce the phase diagram of water from the liquid state down to the supercooled region. Besides it is one of the few water model potentials for which the LLCP has been rigorously proven to exist [62].

To integrate the equation of motion we used a timestep of 1 fs. To deal with electrostatic interactions the Particle–Mesh Ewald method was used. For non-bonded Lennard-Jones interaction, the cutoff was set to 1 nm. Periodic boundary conditions were applied.

The simulations have been performed in the NVT ensemble. To control the temperature we used the velocity rescaling with a stochastic term thermostat [79].

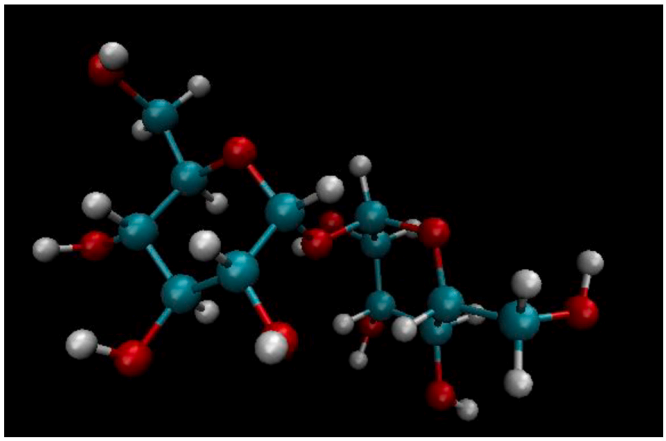

Fig. 1. Representation of the trehalose molecule. The color code for the atoms is red for oxygen, white for hydrogen, and turquoise for carbon.

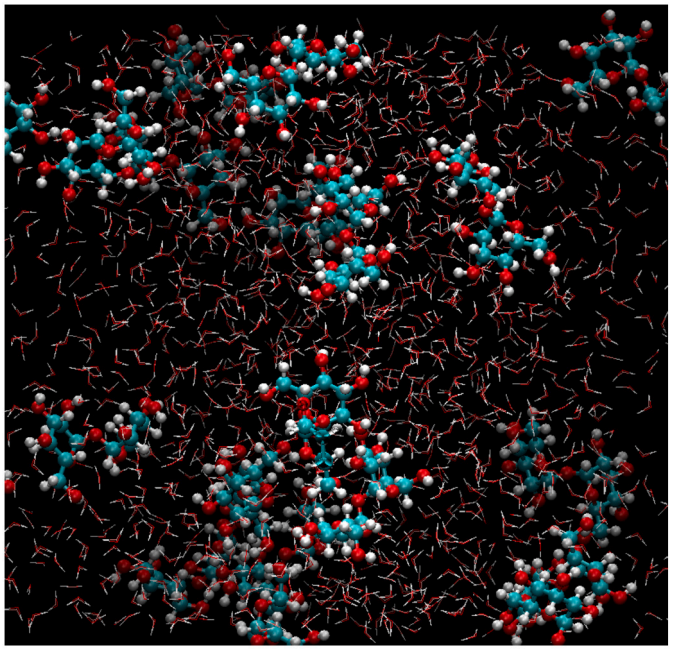

Fig. 2. Blowup of a snapshot of the 20 wt% trehalose aqueous solution simulation box at T = 200 K and ρ = 1100 kg/m^3. The color code for the atoms is red for oxygen, white for hydrogen, and turquoise for carbon. Trehalose is represented with balls and sticks and water is represented with sticks.

For the 20 wt% solutions we simulated the state points for densities from 1180 to 960 kg/m^3 with steps of 10 kg/m^3, and for each density the range of temperatures simulated goes from T = 350 K to T = 160 K, with steps of 10 K for temperatures from 350 K to 300 K and steps of 5 K for lower temperatures. For the 40 wt% solutions the range of densities studied goes from 1280 kg/m^3 to 1060 kg/m^3 with steps of 10 kg/m^3, and for each density the range of temperatures goes from T = 350 K to T = 170 K, with steps of 10 K for temperatures from 350 K to 300 K and steps of 5 K for lower temperatures. We simulated a total of 1518 state points.

For each state point, an equilibration run followed by a production run was made. The simulation times for each state point range from 0.1 ns up to 200 ns for the lowest temperatures.

3. Thermodynamic results

Here we show and analyze the thermodynamic properties of the two trehalose aqueous solutions that result from the behavior of the iso-

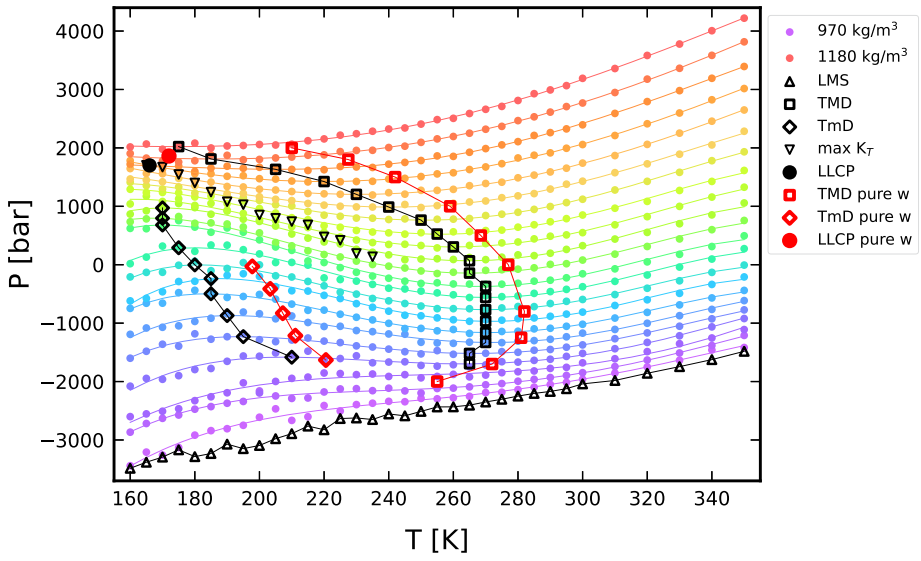

Fig. 3. Isochores for 20 wt% trehalose aqueous solution in the P-T plane as obtained from our MD simulations. Lines are polynomial fits to the simulated state points. The LLCP (black circle), K_T maxima as a proxy of the Widom line (black triangles down), TMD and TmD for the solution (black squares and diamonds), and the limit of mechanical stability line (black triangles up) are also reported. The TMD, TmD and LLCP points for TIP4P/2005 pure water (red squares, red diamonds and red circles respectively), taken from ref. 69 and ref. 62, are also shown for comparison.

chores and the isotherms curves, obtained by reporting in the pressure-temperature and the pressure-density planes the state points calculated from our simulations.

3.1. 20 wt% solution

The state points obtained from the simulations of the 20 wt% in trehalose solution, reported in the isochores P-T plane, are shown in Fig. 3. The lines shown in the figure are fourth-degree polynomial fits to the state points, and each line corresponds to an isochore. From the isochores it is possible to calculate the points of the temperature of maximum density (TMD) line, which correspond to the minima of the isochores. In fact in these minima the coefficient of thermal expansion α_P, defined as

$$\alpha_P = \frac{1}{V}\left(\frac{\partial V}{\partial T}\right)_P = -\frac{1}{\rho}\left(\frac{\partial \rho}{\partial T}\right)_P = K_T\left(\frac{\partial P}{\partial T}\right)_V \quad (1)$$

where K_T is the isothermal compressibility, is equal to 0. α_P changes from positive to negative values for temperatures below the TMD, which means that as the temperature decreases below the TMD at constant pressure the density decreases rather than increases.

We can see that all the isochores, except those corresponding to the four lowest densities, show a minimum in the temperature range analyzed, and all the minima form the TMD line. Some isochores also present a point of relative maximum, and these maxima mark the temperature of minimum density (TmD) line, the line after which the liquid restores the normal behavior. The TMD and TmD lines encompass the density anomaly region, where the density decreases with decreasing temperature at a fixed pressure. The TMD and TmD lines are also drawn in Fig. 3, along with the TMD and TmD lines for pure TIP4P/2005 water [69], shown for comparison. We can see that the TMD and TmD of the solution have a behavior similar to that of pure water but they shift to lower temperatures and lower pressures. The region of density anomaly is therefore moved but similar in size.

In Fig. 3 it is also reported the limit of mechanical stability (LMS) of the liquid metastable phase with respect to the gas phase, which coincides with the lowest isochore plotted. We determined the LMS by decreasing the density. Below the liquid-gas LMS the simulations presented cavitation, i.e. the formation of vapor bubbles, corresponding to a sudden increase in pressure [80].

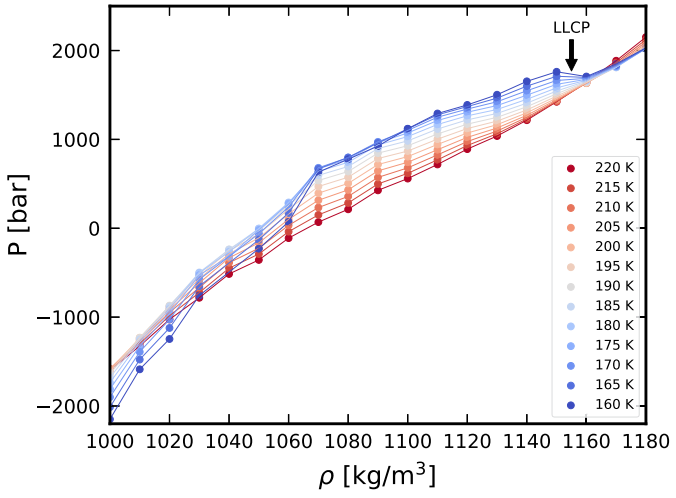

Fig. 4. Isotherms for the 20 wt% trehalose aqueous solution as obtained from our MD simulations, for temperatures from 220 K to 160 K.

From Fig. 3 we can also see that the isochores converge at high pressure and low temperatures. It is possible to estimate the position of the LLCP from the highest temperature crossing point of the isochores. We observe that the isochores corresponding to the densities of 1150 and 1160 kg/m^3 show a crossing at a temperature of about 166 K and a pressure of about 1700 bar, and we highlighted this point in the figure.

In order to better pinpoint the LLCP we reported the state points obtained from the simulations also in the isotherms P-ρ plane, as shown in Fig. 4. We can in fact estimate the location of the LLCP also from the occurrence of a horizontal inflection point in the isotherms, where

$$(\partial P/\partial \rho)_T = (\partial^2 P/\partial \rho^2)_T = 0 \quad (2)$$

We can see that the T = 165 K isotherm shows the only horizontal inflection point of the curves for a density between 1150 and 1160 kg/m^3. Its position is confirmed because it corresponds with our estimated location of the LLCP from the crossing of the isochores.

A further confirmation of the LLCP location can be obtained with the study of the isothermal compressibility K_T. In Fig. 5 we reported the K_T, defined as

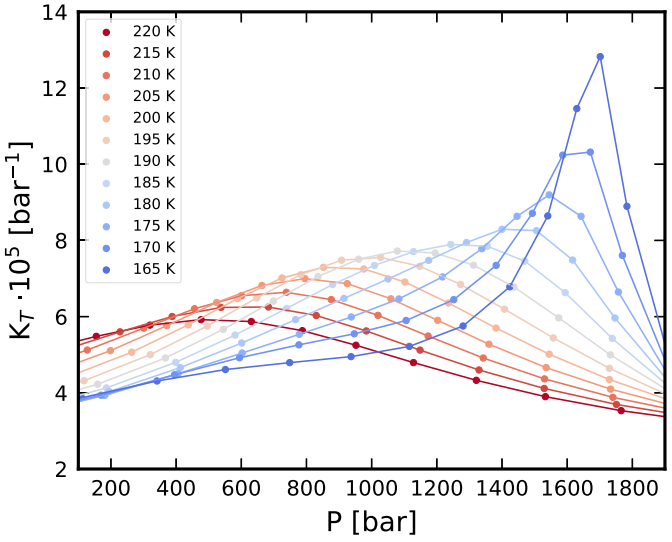

Fig. 5. Isothermal compressibilities for the 20%wt trehalose aqueous solutions, for temperatures from 220 K to 165 K. The compressibilities shown in this paper have been calculated by numerical derivative of an interpolation of the points of the isotherms.

$$K_T = \frac{1}{\rho}\left(\frac{\partial \rho}{\partial P}\right)_T \tag{3}$$

calculated for the 20 wt% solution. We observe that they show well-defined maxima that sharpen as the temperature decreases and as they approach the location of the critical point. The positions of these maxima are also reported in Fig. 3. We see that the line of maxima of the isothermal compressibilities, which can be taken as a proxy of the Widom Line near the critical point, converges to the estimated position of the LLCP, as predicted by the theory of critical phenomena.

From all these results, we estimate the position of the LLCP for the 20 wt% trehalose aqueous solution to be at $T_c = 166$ K and $P_c = 1700$ bar circa. In Fig. 3 we also reported the LLCP of pure water, which was calculated to be at $T_c^{pure} = 172$ K and $P_c^{pure} = 1861$ bar [62]. So there is a decrease in the solution of circa 6 K in temperature and of circa 160 bar in pressure.

3.2. 40 wt% solution

In Fig. 6 we show the state points obtained from the simulations of the 40 wt% solution, reported in the isochores P-T plane. The lines shown are fourth-degree polynomial fits to the state points, and each one corresponds to an isochore. The densities span from 1280 kg/m^3 to 1060 kg/m^3 and the temperatures from T = 350 K to T = 170 K. Also the liquid-gas limit of mechanical stability, which coincides with the isochore at the lowest density, is reported in the figure.

From the minima and the maxima of the isochores we calculated the TMD and TmD lines, and their points are reported in the figure. The minima and maxima of the isochores are way less pronounced for this concentration, indicating a weakening of the density anomaly. The region of the density anomaly is however still present albeit substantially reduced with respect to pure water, whose TMD, TmD and LLCP are also reported in Fig. 6. We note that the reduction is mainly due to a shift with respect to pure water to lower pressures and temperatures of the TMD, while the TmD is only slightly shifted.

The weakening can also be seen from the isotherms, reported in Fig. 7. The region of crossing between the low temperature and high temperature isotherms is much less wide than that of the lower concentration and of pure water.

We can see from Fig. 6 that for this concentration the isochores do not converge and from Fig. 7 that the isotherms do not show a horizontal inflection point, therefore no critical point is observed, at least in the range of temperatures considered.

We calculated also for this concentration the isothermal compressibility K_T, reported in Fig. 8. We can see that the K_T still show maxima points, although they are less pronounced than those of the 20 wt% solution, and after an increase upon decreasing temperature they start to decrease for temperatures below 185 K. This also indicates that in the 40 wt% solution in the range of pressures and temperatures investigated the LLCP is no longer present. The maxima of the K_T are also reported in Fig. 6.

3.3. Comparison of the results of the solutions

To compare the thermodynamic features (TMD, TmD, LLCP, LMS, line of K_T maxima) of the 20 wt% and 40 wt% trehalose aqueous solutions found from our simulations we report these quantities in Fig. 9, along with the TMD, TmD [69] and LLCP [62] for TIP4P/2005 pure water. We report also the TMD and TmD lines for the 20 wt% and 40 wt% trehalose solutions in the $\rho - T$ plane in Fig. 10 as extracted from our isochores analysis. The shift is due to the difference in total density between the different concentrations.

We can see that for the 20 wt% solution the TMD and TmD are shifted to lower temperatures with respect to pure water of about 15 K. The LLCP was found at a temperature $T_c = 166$ K and a pressure $P_c = 1700$ bar, and this location is shifted to lower temperatures and lower pressure with respect to pure water.

In the 40 wt% solution the TMD and TmD are still present, although they are much less wide and the minima and maxima of the isochores are way less pronounced for this solution, indicating a weakening of the density anomaly for this concentration. The TMD line is shifted to even lower temperatures than the 20 wt% one. The TmD moves towards lower temperatures than that of pure water, but to higher or equal temperatures compared to the lower concentration solution, showing that the region of density anomaly has shrunk, and that the shrinkage is especially due to change of location of the TMD line. This is probably due to the fact that the TmD falls in the region where water is more LDL, and therefore less influenced by solutes because of its locally more ordered structure. For the 40 wt% solution the isochores do not converge and therefore no critical point is observed down to the lowest temperature investigated. We also note that the Widom Line, which divides the region where water is more HDL-like (above) from the region more LDL-like (below), has substantially shifted downward for this concentration. This means that the LDL-like region is less favored in the 40 wt% than in the 20 wt% solution and in pure water, since the LMS of pure water, 20 wt% and 40 wt% practically coincide, so that the region where the liquid is more LDL-like has shrunk. We must nonetheless note that the 40 wt% mixture still retains the features that connote the water anomalous behavior.

4. Structural results

We now analyze the structural properties of the solutions by looking at the radial distribution functions (RDFs) $g(r)$.

We start by analyzing the water oxygen - water oxygen (O_w-O_w) RDFs. We compared high densities where in pure water prevails the typical HDL behavior and low densities where in pure water prevails the typical LDL behavior. As high densities we selected $\rho = 1180$ kg/m^3 for the 20 wt% solution, $\rho = 1280$ kg/m^3 for the 40 wt% solution, $\rho = 1100$ kg/m^3 for pure water. All these three densities are well above the LLCP of pure water and of the 20 wt% solution. As low densities we selected $\rho = 1000$ kg/m^3 for the 20 wt% solution, $\rho = 1110$ kg/m^3 for the 40 wt% solution, and $\rho = 900$ kg/m^3 for pure water. All these three densities are well below the LLCP of pure water and of the 20 wt% solution. To best compare different concentrations we chose these particular isochores because they have the best matching similar behavior at low

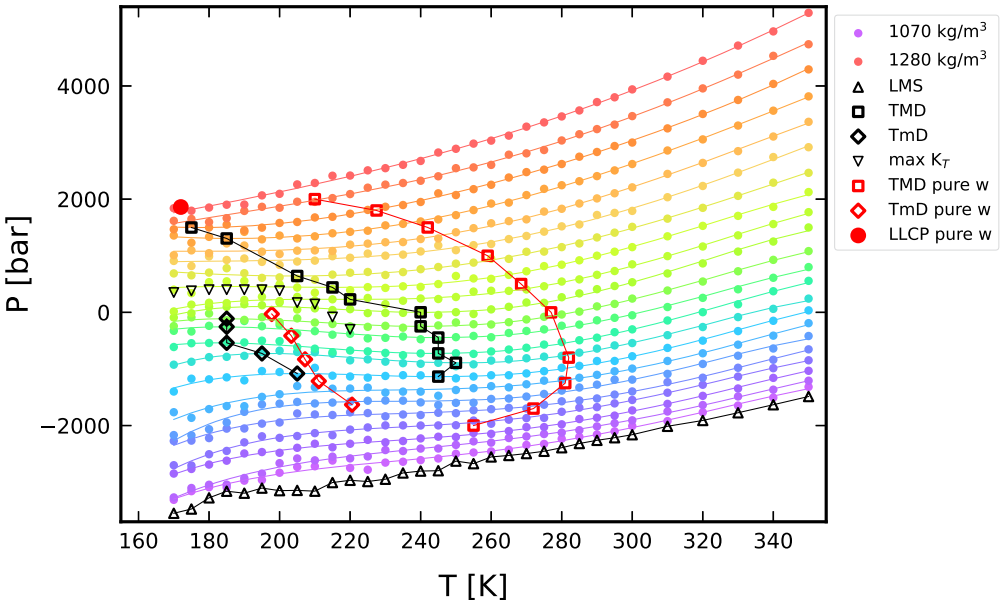

Fig. 6. Isochores for 40 wt% trehalose aqueous solution in the P-T plane as obtained from our MD simulations. Lines are polynomial fits to the simulated state points. The TMD and TmD for the solution (black squares and black diamonds), K_T maxima (black triangles down), and the limit of mechanical stability line (black triangles up) are also reported. The TMD, TmD and LLCP points for pure water (red squares, red diamonds and red circles respectively), taken from ref. 69 and ref. 62, are also shown for comparison.

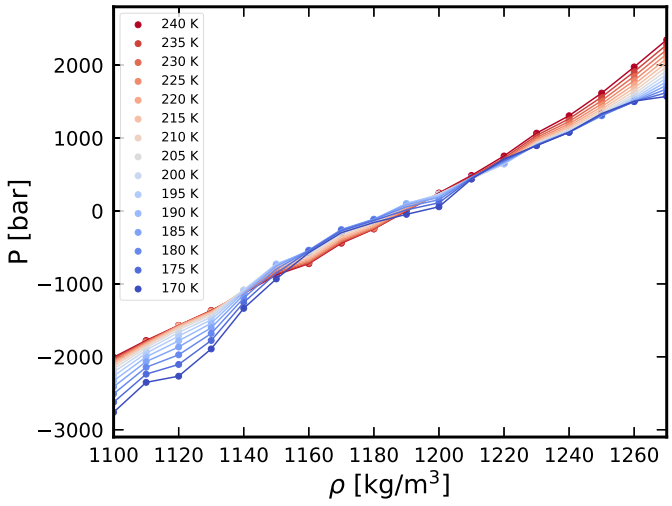

Fig. 7. Isotherms for the 40 wt% trehalose aqueous solution as obtained from our MD simulations, for temperatures from 240 K to 170 K.

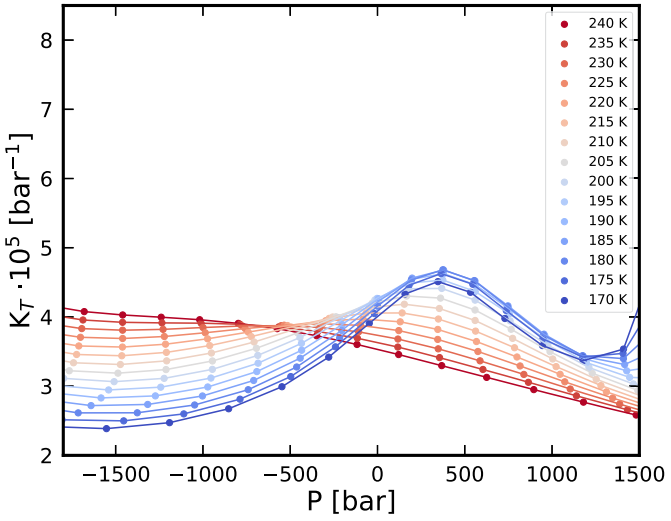

Fig. 8. Isothermal compressibilities for the 40 wt% trehalose aqueous solutions, for temperatures from 240 K to 170 K.

temperatures. Their behavior can be seen in Fig. 11 for both high and low densities.

In Fig. 12 we compare the water oxygen - water oxygen (O_w-O_w) RDFs for the two concentrations and for pure water at high and low densities, for a high temperature, T = 300 K, in the top panel, and a low temperature, T = 170 K, in the bottom panel.

At low temperature, the O_w-O_w RDFs at low densities show a deep first minimum followed by a fairly sharp second peak, whereas at higher densities the first minimum is milder and the second maximum is broader, less peaked, and at a shorter distance with respect to the one for low densities. This indicates a disrupture of hydrogen bonds between the first and the second shell and consequently a collapse of the second shell in the high density liquid (HDL) phase with respect to the low density liquid (LDL) phase, which is more ordered. These are typical characteristics of the O_w-O_w RDFs of the LDL and HDL phases [81]. In these RDFs we observe the main peak around 0.275 nm, and a second peak around 0.45 nm at low density and around 0.43 nm at high density. The first minimum goes from around 0.325 nm to around 0.31 nm upon increasing the density.

In Fig. 13 we plot the O_w-O_w RDFs for both the concentration and densities selected (one each panel), for four selected temperatures each, in order to show how they change from high to low temperatures. By increasing the temperature the peaks of the RDFs become lower but the differences between high and low density are still present at high temperature (T = 300 K): at high density the first minimum and second peak are way less pronounced and placed at lower distances than those at low density.

We can see from these RDFs that even at high concentrations of trehalose water maintains the structural differences between the two liquid high density and low density phases (HDL and LDL), and the structure of water appears not to be affected by the trehalose concentration. The only minor differences between the different concentrations are a higher first and second peak and a more filled first minimum as the concentra-

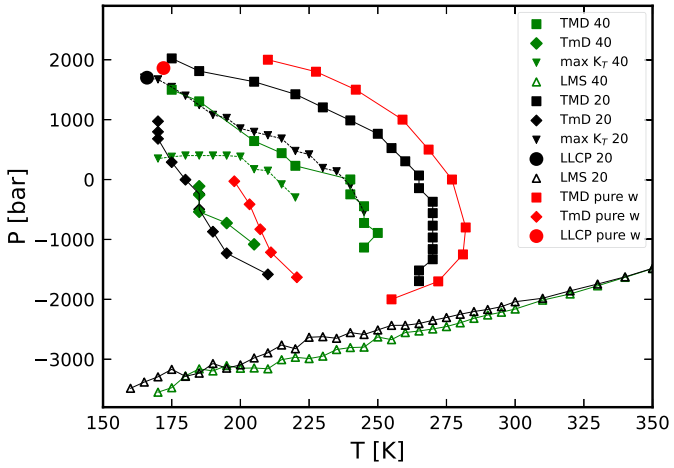

Fig. 9. Comparison of the thermodynamic features (TMD, TmD, LLCP, LMS, line of K_T maxima) between the two trehalose solutions (20 wt% and 40 wt% in trehalose) and pure water.

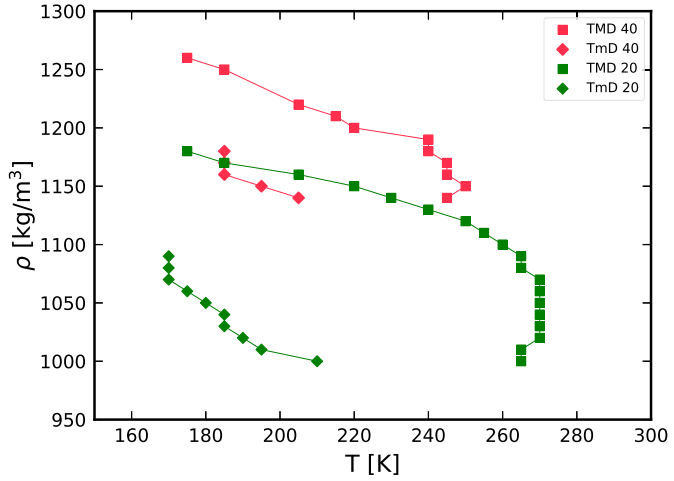

Fig. 10. Comparison of the TMD and TmD lines between the 20 wt% and 40 wt% trehalose solutions in the $\rho - T$ plane, as extracted from our isochores points.

tion increases, for all the densities and temperatures. This indicates that as the concentration of trehalose increases water is more HDL.

In Fig. 14 we show the O_w-O_w first shell coordination numbers at different temperatures as a function of density, calculated from the RDFs using as a cutoff distance the first RDF minimum:

$$N_{coord} = 4\pi\rho \int_0^{r_{min}} g_{OO}(r) r^2 dr \tag{4}$$

For both concentrations, the coordination numbers show an increasing pattern as density increases for high temperatures, with a slope that decreases as the temperature decreases, becoming almost constant at the lower temperature. For the 20 wt% in trehalose solution at T = 300 K the values go from 3.83 at the lower density to 4.66 at the higher density, and at T = 160 K they go from 3.78 to 3.82. Upon increasing the concentration the curves have similar slopes but move downward, meaning that more water molecules solvate the trehalose molecules of the solutions. For the 40 wt% solution the values of the coordination number go from 3.52 at the lower density to 4.28 at the higher density at T = 300 K, and from 3.48 to 3.52 at T = 170 K.

In order to inquire on how water molecules solvate the trehalose in Fig. 15 we plot the trehalose oxygen - water oxygen (O_t-O_w) RDFs for the two concentrations at high and low densities and temperatures,

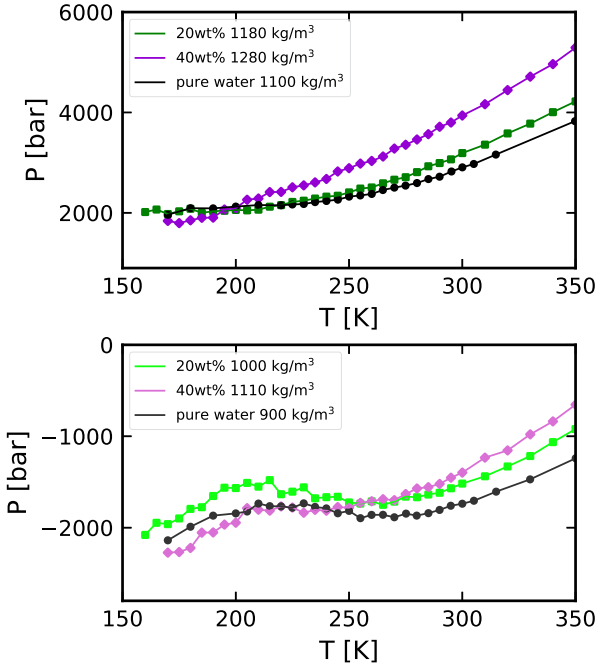

Fig. 11. Isochores selected as best matching at low temperatures for the RDFs calculation at high density (top panel) and low density (bottom panel) for pure water, the 20 wt%, and the 40 wt% solutions.

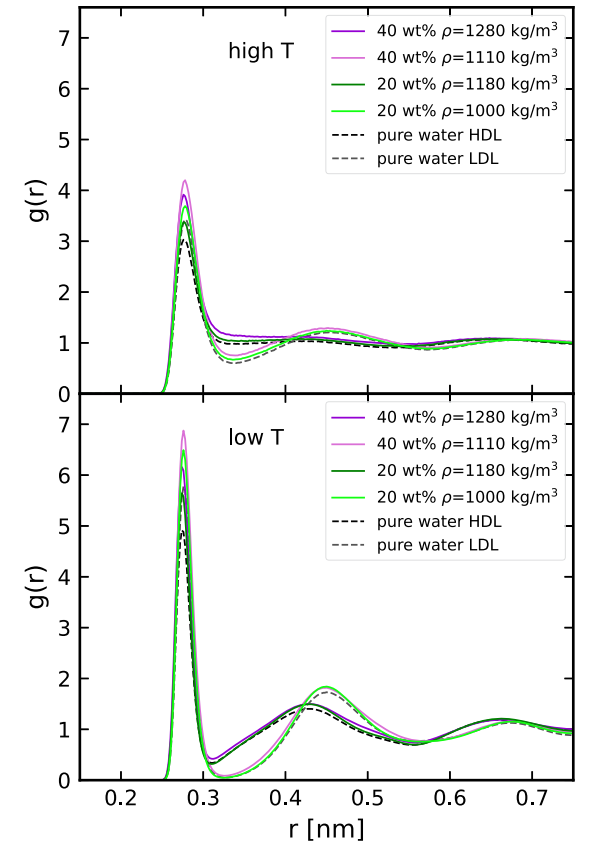

Fig. 12. O_w-O_w RDFs for the two solutions at high and low densities (1280 kg/m^3 and 1110 kg/m^3 respectively for the 40 wt% solution, and 1180 kg/m^3 and 1000 kg/m^3 for the 20 wt% solution). Pure water O_w-O_w RDFs at high and low densities (1100 kg/m^3 and 900 kg/m^3) are also reported. Top panel: RDFs at high temperature (T = 300 K). Bottom panel: low temperature (T = 170 K).

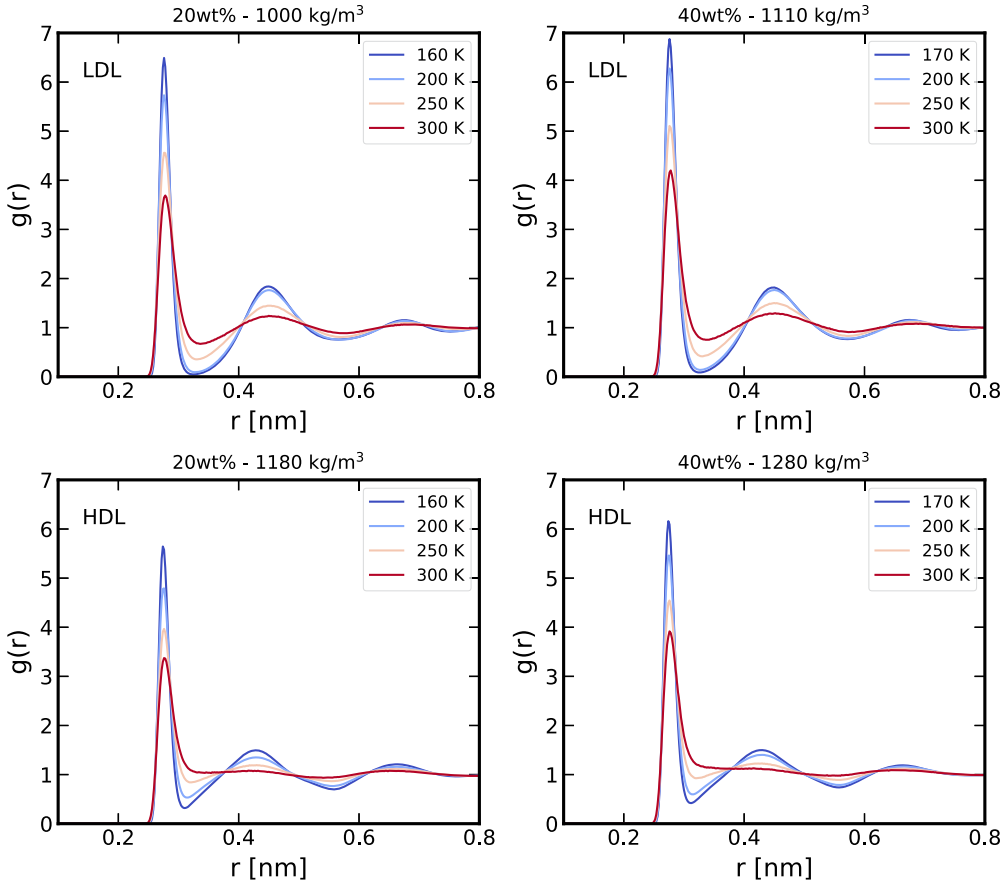

Fig. 13. O_w-O_w RDFs. In the left panels we report the RDFs for the 20 wt% solution and in the right panels for the 40 wt% solution, in the top panels for low densities and in the bottom panels for high densities. The RDFs for each density and concentration are reported from high to low temperature.

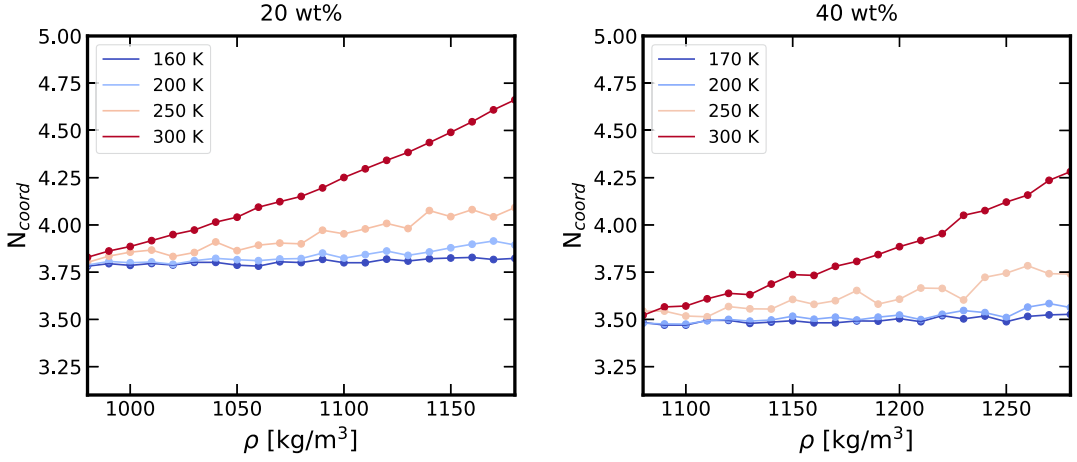

Fig. 14. O_w-O_w first shell coordination numbers for the two solutions (left panel: 20 wt% and right panel: 40 wt%) as functions of density for different temperatures.

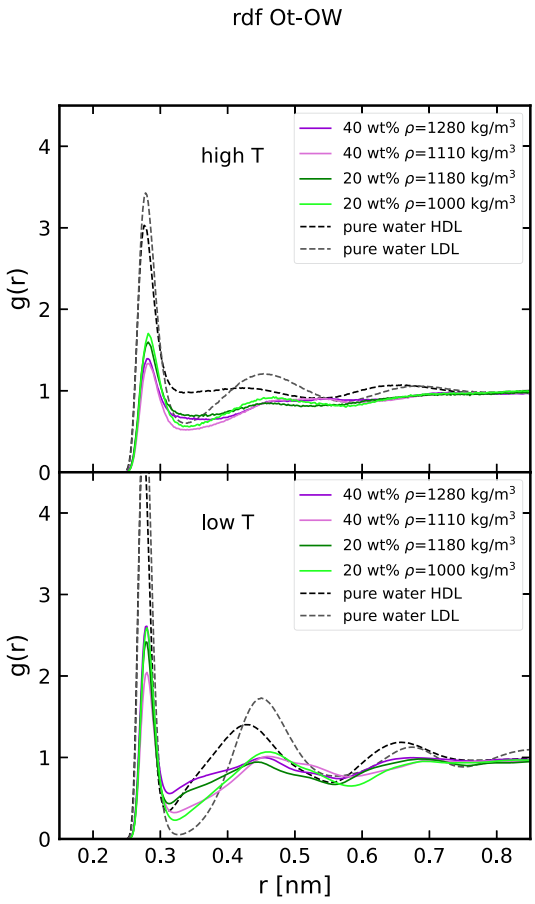

Fig. 15. Trehalose oxygen - water oxygen RDFs of the two solutions (20 and 40 wt% in trehalose), compared with pure water oxygen - oxygen RDFs. First panel: RDFs at high temperature (T = 300 K) at high and low densities. Second panel: RDFs at low temperature (T = 170 K) for the two solutions and for at high and low densities.

compared with the O_w-O_w RDFs. To compute these RDFs we selected as oxygen atoms of the trehalose molecules the ones in the OH groups. We observe that at low temperatures at both high and low densities water tends to be more HDL-like at the interface with trehalose, and this is even more evident in the solution with the higher concentration because these RDFs present a more filled first minimum. At low temperatures therefore trehalose appears to favor the high density phase of water.

We computed also the average number of all water molecules in the first hydration layer around a trehalose molecule, and we report the results in Fig. 16. We selected as a cutoff distance of the water molecules with the atoms of the trehalose molecules 0.32 nm, which coincides with the first minimum of the trehalose oxygen - water oxygen RDFs, as it can be seen in Fig. 15.

The number of water molecules solvating the trehalose shows an increase as density increases. This indicates that water at lower densities, when it is more LDL-like, tends to exclude solutes more, while at high densities, when it is more HDL-like, it tends to solvate trehalose more. Water is more LDL-like for low densities and/or low temperatures. We observe that for both concentrations the average number of water molecules around each trehalose molecule does not depend on temperature, except for the lowest densities where the two lowest temperatures, T = 200 K and T = 160 K for the 20 wt% solution and T = 170 K for the 40 wt% solution, present a slightly lower number of water molecules around the trehalose.

In the solution with a higher concentration of trehalose the average number of water solvating the disaccharide is lower than in the solution with a lower concentration. This can be due to a greater tendency for trehaloses to aggregate when present in greater quantities in the solution, thus excluding some of the water molecules from the first layer.

A tendency to aggregate is been observed in Ref. 14. Overall the number of water molecules solvating a trehalose molecule goes from around 20 to around 29 for the 20 wt% solution and from around 19 to around 26 for the 40 wt% solution. We also note that in the 40 wt% solution almost all water molecules solvate the trehalose at high density.

5. Conclusions

We have studied through molecular dynamics simulations trehalose and water solutions (20 wt% and 40 wt% in trehalose), to analyze their thermodynamic and structural properties. Trehalose is a well-known cryoprotectant. We used for water in the simulation the TIP4P/2005 potential. We simulated state points for a wide span of densities and temperatures up to the deeply supercooled region.

From the thermodynamic analysis we deduced the phase diagram of the liquid phase in the normal and the supercooled liquid region. We saw that in the 20 wt% solution the density anomaly is still present, the isochores show well defined minima and maxima, and the TMD line is shifted to lower temperatures than that of pure water of about 10 K. We can also observe that the isochores converge and the isotherms show a horizontal inflection point The line of K_T maxima also points towards this region. These observations indicate the presence of a LLCP in the 20 wt% at T_c = 166 K and a pressure P_c = 1700 bar, shifted at lower temperatures and slightly lower pressures than that of pure water [62].

Also for the 40 wt% solution the density anomaly is still present, although it is much less wide and the minima and maxima of the isochores are way less pronounced for this solution. The TMD line is shifted to even lower temperatures with respect to the pure water one, and the region inside the TMD curve is substantially shrunk. Furthermore, the K_T maxima for this concentration are less pronounced than those of the 20 wt% solution and decrease for lower temperatures, indicating a weakening of these anomalies. For this concentration the isochores do not converge and therefore no critical point is observed.

Nonetheless overall water anomalies are still present in the trehalose aqueous solutions investigated, also for the highest concentration, indicating that water anomalous behavior is important also when water is mixed with trehalose.

We note that the anomaly in K_T that we studied and that is directly related to the Widom line and to the LLCP, still persists in the 40 wt% solution, showing a weaker anomalous behavior.

We also note that in pure TIP4P/2005 water [82–84], similar to other water potentials [85–91], the Widom line practically coincides with the dynamical fragile to strong crossover. We plan to study this phenomenon also in this system in the near future.

Our results of the location of LLCP in the 20 wt% solution is compatible with the experimental estimate of the LLCP by Suzuki [48], although the comparison cannot be precise since its concentration falls in between our two.

From our study of RDFs we see that HDL and LDL structures are very similar to pure water. In order to have more information on the microscopic local structure a future study on local structure indicators could give more information [92–94].

The presence of trehalose appears to favor the high-density phase of water, as it is evident from the analysis of the water oxygen - water oxygen RDFs, which present a more filled first minimum. It is also evident from the characteristics of the solvation shell, and from the shift to lower pressures of the LLCP, which indicates a shrinkage of the LDL region. In fact, for temperatures below the LLCP, the coexistence line separates the HDL and LDL phases, while above the LLCP the Widom line separates the phase diagram in a region more HDL-like and a region more LDL-like.

The favoring of the HDL local structure can be linked to the cryoprotectant properties of trehalose of preventing crystallization, since nucleation is favored in the low density liquid [26].

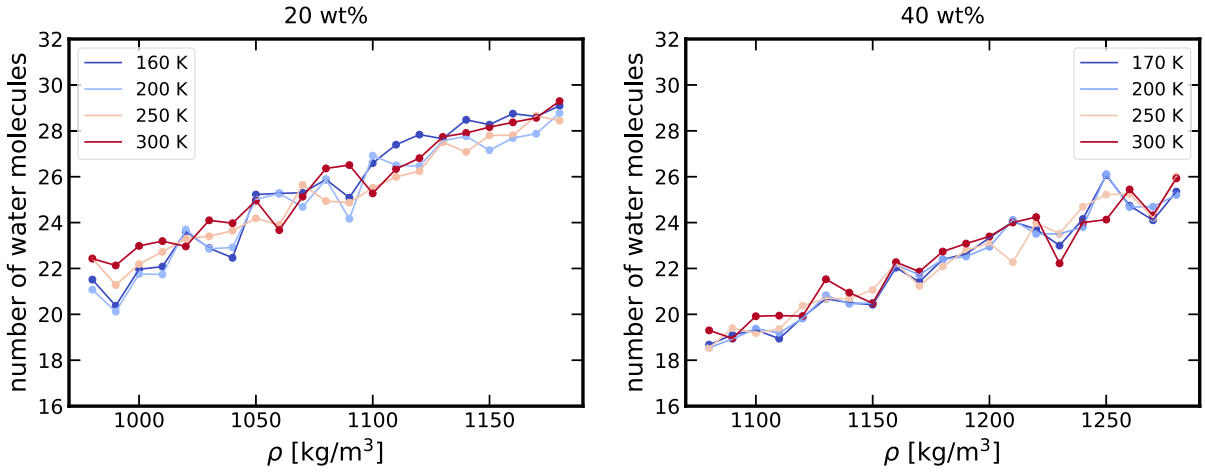

Fig. 16. Average number of water molecules in the first hydration layer around a trehalose molecule for the two concentrations (left panel: 20 wt% and right panel: 40 wt%) as a function of density, for different temperatures.

CRediT authorship contribution statement

Leonardo Perin: Writing – review & editing, Writing – original draft, Visualization, Validation, Methodology, Investigation, Formal analysis, Data curation. **Paola Gallo:** Writing – review & editing, Writing – original draft, Visualization, Validation, Supervision, Project administration, Methodology, Investigation, Funding acquisition, Formal analysis, Data curation, Conceptualization.

Declaration of competing interest

The authors declare that they have no known competing financial interests or personal relationships that could have appeared to influence the work reported in this paper.

Data availability

Data will be made available on request.

References

[1] L.M. Crowe, D.S. Reid, J.H. Crowe, Is trehalose special for preserving dry biomaterials?, Biophys. J. 71 (4) (1996) 2087–2093, https://doi.org/10.1016/S0006-3495(96)79407-9.
[2] N.K. Jain, I. Roy, Effect of trehalose on protein structure, Protein Sci. 18 (1) (2009) 24–36, https://doi.org/10.1002/pro.3.
[3] J.K. Kaushik, R. Bhat, Why is trehalose an exceptional protein stabilizer?: an analysis of the thermal stability of proteins in the presence of the compatible osmolyte trehalose, J. Biol. Chem. 278 (29) (2003) 26458–26465, https://doi.org/10.1074/jbc.M300815200.
[4] M. Heyden, E. Bründermann, U. Heugen, G. Niehues, D.M. Leitner, M. Havenith, Long-range influence of carbohydrates on the solvation dynamics of water—answers from terahertz absorption measurements and molecular modeling simulations, J. Am. Chem. Soc. 130 (17) (2008) 5773–5779, https://doi.org/10.1021/ja0781083.
[5] L. Cordone, G. Cottone, A. Cupane, A. Emanuele, S. Giuffrida, M. Levantino, Proteins in saccharides matrices and the trehalose peculiarity: biochemical and biophysical properties, Curr. Org. Chem. 19 (17) (2015) 1684–1706, https://doi.org/10.2174/1385272819666150429232426.
[6] D. Corradini, E.G. Strekalova, H. Stanley, P. Gallo, Microscopic mechanism of protein cryopreservation in an aqueous solution with trehalose, Sci. Rep. 3 (1218) (2013), https://doi.org/10.1038/srep01218.
[7] P.S. Belton, A.M. Gil, Ir and raman spectroscopic studies of the interaction of trehalose with hen egg white lysozyme, Biopolymers 34 (7) (1994) 957–961, https://doi.org/10.1002/bip.360340713.
[8] S. Giuffrida, L. Cordone, G. Cottone, Bioprotection can be tuned with a proper protein/saccharide ratio: the case of solid amorphous matrices, J. Phys. Chem. B 122 (37) (2018) 8642–8653, https://doi.org/10.1021/acs.jpcb.8b05098.
[9] S. Corezzi, M. Paolantoni, P. Sassi, A. Morresi, D. Fioretto, L. Comez, Trehalose-induced slowdown of lysozyme hydration dynamics probed by edls spectroscopy, J. Chem. Phys. 151 (1) (2019) 015101, https://doi.org/10.1063/1.5099588.
[10] S. Corezzi, B. Bracco, P. Sassi, M. Paolantoni, L. Comez, Protein hydration in a bioprotecting mixture, Life 11 (10) (2021), https://doi.org/10.3390/life11100995.
[11] B.P. Rosi, L. Tavagnacco, L. Comez, P. Sassi, M. Ricci, E. Buratti, M. Bertoldo, C. Petrillo, E. Zaccarelli, E. Chiessi, S. Corezzi, Thermoresponsivity of poly(n-isopropylacrylamide) microgels in water-trehalose solution and its relation to protein behavior, J. Colloid Interface Sci. 604 (2021) 705–718, https://doi.org/10.1016/j.jcis.2021.07.006.
[12] M. Zanatta, L. Tavagnacco, E. Buratti, M. Bertoldo, F. Natali, E. Chiessi, A. Orecchini, E. Zaccarelli, Evidence of a low-temperature dynamical transition in concentrated microgels, Sci. Adv. 4 (9) (2018) eaat5895, https://doi.org/10.1126/sciadv.aat5895.
[13] G. Camisasca, M. De Marzio, P. Gallo, Effect of trehalose on protein cryoprotection: insights into the mechanism of slowing down of hydration water, J. Chem. Phys. 153 (2020) 224503, https://doi.org/10.1063/5.0033526.
[14] A. Iorio, G. Camisasca, M. Rovere, P. Gallo, Characterization of hydration water in supercooled water-trehalose solutions: the role of the hydrogen bonds network, J. Chem. Phys. 151 (4) (2019) 044507, https://doi.org/10.1063/1.5108579.
[15] A. Iorio, G. Camisasca, P. Gallo, Slow dynamics of hydration water and the trehalose dynamical transition, J. Mol. Liq. 282 (2019) 617–625, https://doi.org/10.1016/j.molliq.2019.02.088.
[16] A. Magno, P. Gallo, Understanding the mechanisms of bioprotection: a comparative study of aqueous solutions of trehalose and maltose upon supercooling, J. Phys. Chem. Lett. 2 (9) (2011) 977–982, https://doi.org/10.1021/jz200256q.
[17] M. Paolantoni, L. Comez, M.E. Gallina, P. Sassi, F. Scarponi, D. Fioretto, A. Morresi, Light scattering spectra of water in trehalose aqueous solutions: evidence for two different solvent relaxation processes, J. Phys. Chem. B 113 (22) (2009) 7874–7878, https://doi.org/10.1021/jp9004983.
[18] A. Lerbret, P. Bordat, F. Affouard, M. Descamps, F. Migliardo, How homogeneous are the trehalose, maltose, and sucrose water solutions? An insight from molecular dynamics simulations, J. Phys. Chem. B 109 (21) (2005) 11046–11057, https://doi.org/10.1021/jp0468657.
[19] A. Lerbret, F. Affouard, P. Bordat, A. Hédoux, Y. Guinet, M. Descamps, Slowing down of water dynamics in disaccharide aqueous solutions, J. Non-Cryst. Solids 357 (2) (2011) 695–699, https://doi.org/10.1016/j.jnoncrysol.2010.05.092.
[20] L. Lupi, L. Comez, M. Paolantoni, D. Fioretto, B.M. Ladanyi, Dynamics of biological water: insights from molecular modeling of light scattering in aqueous trehalose solutions, J. Phys. Chem. B 116 (25) (2012) 7499–7508, https://doi.org/10.1021/jp301988f.
[21] S. Giuffrida, G. Cottone, L. Cordone, The water association band as a marker of hydrogen bonds in trehalose amorphous matrices, Phys. Chem. Chem. Phys. 19 (2017) 4251–4265, https://doi.org/10.1039/C6CP06848K.
[22] S. Giuffrida, A. Cupane, G. Cottone, "Water association" band in saccharide amorphous matrices: role of residual water on bioprotection, Int. J. Mol. Sci. 22 (5) (2021), https://doi.org/10.3390/ijms22052496.
[23] C.H. Robinson, Cold adaptation in Arctic and Antarctic fungi, New Phytol. 151 (2) (2001) 341–353, https://doi.org/10.1046/j.1469-8137.2001.00177.x.
[24] G.M. Wang, A.D.J. Haymet, Trehalose and other sugar solutions at low temperature: modulated differential scanning calorimetry (mdsc), J. Phys. Chem. B 102 (27) (1998) 5341–5347, https://doi.org/10.1021/jp980942e.
[25] J.L. Green, C.A. Angell, Phase relations and vitrification in saccharide-water solutions and the trehalose anomaly, J. Phys. Chem. 93 (8) (1989) 2880–2882, https://doi.org/10.1021/j100345a006.
[26] P. Gallo, K. Amann-Winkel, C.A. Angell, M.A. Anisimov, F. Caupin, C. Chakravarty, E. Lascaris, T. Loerting, A.Z. Panagiotopoulos, J. Russo, J.A. Sellberg, H.E. Stanley, H. Tanaka, C. Vega, L. Xu, L.G.M. Pettersson, Water: a tale of two liquids, Chem. Rev. 116 (13) (2016) 7463–7500, https://doi.org/10.1021/acs.chemrev.5b00750.

[27] P.G. Debenedetti, Supercooled and glassy water, J. Phys. Condens. Matter 15 (45) (2003) R1669–R1726, https://doi.org/10.1088/0953-8984/15/45/R01.
[28] P.G. Debenedetti, H.E. Stanley, Supercooled and glassy water, Phys. Today 56 (6) (2003) 40–46, https://doi.org/10.1063/1.1595053.
[29] P.G. Debenedetti, Metastable Liquids: Concepts and Principles, Princeton University Press, 1997.
[30] P. Gallo, H.E. Stanley, Supercooled water reveals its secrets, Science 358 (6370) (2017) 1543–1544, https://doi.org/10.1126/science.aar3575.
[31] P. Gallo, J. Bachler, L.E. Bove, R. Böhmer, G. Camisasca, L.E. Coronas, H.R. Corti, I. de Almeida Ribeiro, M. de Koning, G. Franzese, V. Fuentes-Landete, C. Gainaru, T. Loerting, J.M. Montes de Oca, P.H. Poole, M. Rovere, F. Sciortino, C.M. Tonauer, G.A. Appignanesi, Advances in the study of supercooled water, Eur. Phys. J. E 44 (11) (2021) 143, https://doi.org/10.1140/epje/s10189-021-00139-1.
[32] J. Errington, P. Debenedetti, Relationship between structural order and the anomalies of liquid water, Nature 409 (2001) 318–321, https://doi.org/10.1038/35053024.
[33] C.A. Angell, H. Kanno, Density maxima in high-pressure supercooled water and liquid silicon dioxide, Science 193 (4258) (1976) 1121–1122, https://doi.org/10.1126/science.193.4258.1121.
[34] F. Mallamace, C. Branca, M. Broccio, C. Corsaro, C.-Y. Mou, S.-H. Chen, The anomalous behavior of the density of water in the range 30 k < t < 373 k, Proc. Natl. Acad. Sci. USA 104 (47) (2007) 18387–18391, https://doi.org/10.1073/pnas.0706504104.
[35] D. Liu, Y. Zhang, C.-C. Chen, C.-Y. Mou, P.H. Poole, S.-H. Chen, Observation of the density minimum in deeply supercooled confined water, Proc. Natl. Acad. Sci. USA 104 (23) (2007) 9570–9574, https://doi.org/10.1073/pnas.0701352104.
[36] R.J. Speedy, C.A. Angell, Isothermal compressibility of supercooled water and evidence for a thermodynamic singularity at -45°c, J. Chem. Phys. 851 (65) (1976), https://doi.org/10.1063/1.433153.
[37] H. Kanno, C.A. Angell, Water: anomalous compressibilities to 1.9 kbar and correlation with supercooling limits, J. Chem. Phys. 70 (9) (1979) 4008–4016, https://doi.org/10.1063/1.438021.
[38] K. Kim, A. Späh, H. Pathak, F. Perakis, D. Mariedahl, K. Amann-Winkel, J. Sellberg, J. Lee, S. Kim, J. Park, K. Nam, T. Katayama, A. Nilsson, Maxima in the thermodynamic response and correlation functions of deeply supercooled water, Science 358 (6370) (2017) 1589–1593, https://doi.org/10.1126/science.aap8269.
[39] C.A. Angell, W.J. Sichina, M. Oguni, Heat capacity of water at extremes of supercooling and superheating, J. Phys. Chem. 86 (6) (1982) 998–1002, https://doi.org/10.1021/j100395a032.
[40] O. Mishima, H. Stanley, The relationship between liquid, supercooled and glassy water, Nature 396 (1998) 329–335, https://doi.org/10.1038/24540.
[41] K. Winkel, E. Mayer, T. Loerting, Equilibrated high-density amorphous ice and its first-order transition to the low-density form, J. Phys. Chem. B 115 (48) (2011) 14141–14148, https://doi.org/10.1021/jp203985w.
[42] K. Winkel, M.S. Elsaesser, E. Mayer, T. Loerting, Water polyamorphism: reversibility and (dis)continuity, J. Chem. Phys. 128 (4) (2008) 044510, https://doi.org/10.1063/1.2830029.
[43] P.H. Poole, F. Sciortino, U. Essmann, H.E. Stanley, Phase behaviour of metastable water, Nature 360 (1992) 324–328, https://doi.org/10.1038/360324a0.
[44] Y. Suzuki, O. Mishima, Experimentally proven liquid-liquid critical point of dilute glycerol-water solution at 150 k, J. Chem. Phys. 141 (9) (2014) 094505, https://doi.org/10.1063/1.4894416.
[45] O. Mishima, H. Stanley, Decompression-induced melting of ice iv and the liquid–liquid transition in water, Nature 392 (1998) 164–168, https://doi.org/10.1038/32386.
[46] S. Woutersen, B. Ensing, M. Hilbers, Z. Zhao, C.A. Angell, A liquid-liquid transition in supercooled aqueous solution related to the hda-lda transition, Science 359 (6380) (2018) 1127–1131, https://doi.org/10.1126/science.aao7049.
[47] K.H. Kim, K. Amann-Winkel, N. Giovambattista, A. Späh, F. Perakis, H. Pathak, M.L. Parada, C. Yang, D. Mariedahl, T. Eklund, T.J. Lane, S. You, S. Jeong, M. Weston, J.H. Lee, I. Eom, M. Kim, J. Park, S.H. Chun, P.H. Poole, A. Nilsson, Experimental observation of the liquid-liquid transition in bulk supercooled water under pressure, Science 370 (6519) (2020) 978–982, https://doi.org/10.1126/science.abb9385.
[48] Y. Suzuki, Direct observation of reversible liquid–liquid transition in a trehalose aqueous solution, Proc. Natl. Acad. Sci. 119 (5) (2022) e2113411119, https://doi.org/10.1073/pnas.2113411119.
[49] L. Xu, P. Kumar, S.V. Buldyrev, S.-H. Chen, P.H. Poole, F. Sciortino, H.E. Stanley, Relation between the widom line and the dynamic crossover in systems with a liquid-liquid phase transition, Proc. Natl. Acad. Sci. USA 102 (46) (2005) 16558–16562, https://doi.org/10.1073/pnas.0507870102.
[50] G. Franzese, H. Stanley, The widom line of supercooled water, J. Phys. Condens. Matter 19 (2007) 205126–16, https://doi.org/10.1088/0953-8984/19/20/205126.
[51] J.L.F. Abascal, C. Vega, Widom line and the liquid–liquid critical point for the tip4p/2005 water model, J. Chem. Phys. 133 (23) (2010) 234502, https://doi.org/10.1063/1.3506860.
[52] P. Gallo, M. Rovere, Physics of Liquid Matter, Springer, 2021.
[53] H.J.C. Berendsen, J.R. Grigera, T.P. Straatsma, The missing term in effective pair potentials, J. Phys. Chem. 91 (24) (1987) 6269–6271, https://doi.org/10.1021/j100308a038.
[54] G.R. Medders, V. Babin, F. Paesani, Development of a “first-principles” water potential with flexible monomers. iii. liquid phase properties, J. Chem. Theory Comput. 10 (8) (2014) 2906–2910, https://doi.org/10.1021/ct5004115.
[55] F. Paesani, Getting the right answers for the right reasons: toward predictive molecular simulations of water with many-body potential energy functions, Acc. Chem. Res. 49 (9) (2016) 1844–1851, https://doi.org/10.1021/acs.accounts.6b00285.
[56] S.K. Reddy, S.C. Straight, P. Bajaj, C. Huy Pham, M. Riera, D.R. Moberg, M.A. Morales, C. Knight, A.W. Götz, F. Paesani, On the accuracy of the mb-pol many-body potential for water: interaction energies, vibrational frequencies, and classical thermodynamic and dynamical properties from clusters to liquid water and ice, J. Chem. Phys. 145 (19) (2016) 194504, https://doi.org/10.1063/1.4967719.
[57] E.R. Pinnick, S. Erramilli, F. Wang, Predicting the melting temperature of ice-ih with only electronic structure information as input, J. Chem. Phys. 137 (1) (2012) 014510, https://doi.org/10.1063/1.4731693.
[58] J.C. Palmer, F. Martelli, Y. Liu, R. Car, A.Z. Panagiotopoulos, P.G. Debenedetti, Metastable liquid-liquid transition in a molecular model of water, Nature 510 (2014) 385–388, https://doi.org/10.1038/nature13405.
[59] F. Sciortino, I. Saika-Voivod, P.H. Poole, Study of the st2 model of water close to the liquid–liquid critical point, Phys. Chem. Chem. Phys. 13 (2011) 19759–19764, https://doi.org/10.1039/C1CP22316J.
[60] T.A. Kesselring, G. Franzese, S.V. Buldyrev, H.J. Herrmann, H.E. Stanley, Nanoscale dynamics of phase flipping in water near its hypothesized liquid-liquid critical point, Sci. Rep. 2 (2012) 474, https://doi.org/10.1038/srep00474.
[61] J.C. Palmer, R. Car, P.G. Debenedetti, The liquid–liquid transition in supercooled st2 water: a comparison between umbrella sampling and well-tempered metadynamics, Faraday Discuss. 167 (2013) 77–94, https://doi.org/10.1039/C3FD00074E.
[62] P.G. Debenedetti, F. Sciortino, G.H. Zerze, Second critical point in two realistic models of water, Science 369 (6501) (2020) 289–292, https://doi.org/10.1126/science.abb9796.
[63] P. Gallo, F. Sciortino, Ising universality class for the liquid-liquid critical point of a one component fluid: a finite-size scaling test, Phys. Rev. Lett. 109 (2012) 177801, https://doi.org/10.1103/PhysRevLett.109.177801.
[64] J. Weis, F. Sciortino, A.Z. Panagiotopoulos, P.G. Debenedetti, Liquid–liquid criticality in the wail water model, J. Chem. Phys. 157 (2) (2022) 024502, https://doi.org/10.1063/5.0099520.
[65] J.L.F. Abascal, C. Vega, A general purpose model for the condensed phases of water: Tip4p/2005, J. Chem. Phys. 123 (23) (2005) 234505, https://doi.org/10.1063/1.2121687.
[66] C. Vega, J.L.F. Abascal, Simulating water with rigid non-polarizable models: a general perspective, Phys. Chem. Chem. Phys. 13 (2011) 19663–19688, https://doi.org/10.1039/C1CP22168J.
[67] H.L. Pi, J.L. Aragones, C. Vega, E.G. Noya, J.L. Abascal, M.A. Gonzalez, C. McBride, Anomalies in water as obtained from computer simulations of the tip4p/2005 model: density maxima, and density, isothermal compressibility and heat capacity minima, Mol. Phys. 107 (4–6) (2009) 365–374, https://doi.org/10.1080/00268970902784926.
[68] J.V.L. Valle, B.H.S. Mendonça, M.C. Barbosa, H. Chacham, E.E. de Moraes, Accuracy of tip4p/2005 and spc/fw water models, J. Phys. Chem. B 128 (4) (2024) 1091–1097, https://doi.org/10.1021/acs.jpcb.3c07044.
[69] M.A. González, C. Valeriani, F. Caupin, J.L.F. Abascal, A comprehensive scenario of the thermodynamic anomalies of water using the tip4p/2005 model, J. Chem. Phys. 145 (5) (2016) 054505, https://doi.org/10.1063/1.4960185.
[70] D. Corradini, M. Rovere, P. Gallo, A route to explain water anomalies from results on an aqueous solution of salt, J. Chem. Phys. 132 (13) (2010) 134508, https://doi.org/10.1063/1.3376776.
[71] D. Corradini, P. Gallo, Liquid–liquid coexistence in nacl aqueous solutions: a simulation study of concentration effects, J. Phys. Chem. B 115 (48) (2011) 14161–14166, https://doi.org/10.1021/jp2045977.
[72] D. Corradini, Z. Su, H.E. Stanley, P. Gallo, A molecular dynamics study of the equation of state and the structure of supercooled aqueous solutions of methanol, J. Chem. Phys. 137 (18) (2012) 184503, https://doi.org/10.1063/1.4767060.
[73] L. Perin, P. Gallo, Phase diagram of aqueous solutions of licl: a study of concentration effects on the anomalies of water, J. Phys. Chem. B 127 (20) (2023) 4613–4622, https://doi.org/10.1021/acs.jpcb.3c00703.
[74] P. La Francesca, P. Gallo, Supercooled solutions of sodium perchlorate in tip4p/2005 water: the effect of martian solutes on thermodynamics and structure, J. Chem. Phys. 159 (12) (2023) 124501, https://doi.org/10.1063/5.0168587.
[75] D. Corradini, S.V. Buldyrev, P. Gallo, H.E. Stanley, Effect of hydrophobic solutes on the liquid-liquid critical point, Phys. Rev. E 81 (2010) 061504, https://doi.org/10.1103/PhysRevE.81.061504.
[76] M.J. Abraham, T. Murtola, R. Schulz, S. Páll, J.C. Smith, B. Hess, E. Lindahl, Gromacs: high performance molecular simulations through multi-level parallelism from laptops to supercomputers, SoftwareX 1–2 (2015) 19–25, https://doi.org/10.1016/j.softx.2015.06.001.
[77] O. Guvench, S.N. Greene, G. Kamath, J.W. Brady, R.M. Venable, R.W. Pastor, A.D. Mackerell Jr, Additive empirical force field for hexopyranose monosaccharides, J. Comput. Chem. 29 (15) (2008) 2543–2564, https://doi.org/10.1002/jcc.21004.
[78] O. Guvench, E. Hatcher, R.M. Venable, R.W. Pastor, A.D.J. MacKerell, Charmm additive all-atom force field for glycosidic linkages between hexopyranoses, J. Chem. Theory Comput. 5 (9) (2009) 2353–2370, https://doi.org/10.1021/ct900242e.

[79] G. Bussi, D. Donadio, M. Parrinello, Canonical sampling through velocity rescaling, J. Chem. Phys. 126 (1) (2007) 014101, https://doi.org/10.1063/1.2408420.
[80] E. Lascaris, The effect of intra-molecular bonds on the liquid–liquid critical point in modified-wac models, J. Chem. Phys. 157 (20) (2022) 204501, https://doi.org/10.1063/5.0123159.
[81] A.K. Soper, M.A. Ricci, Structures of high-density and low-density water, Phys. Rev. Lett. 84 (2000) 2881–2884, https://doi.org/10.1103/PhysRevLett.84.2881.
[82] M. De Marzio, G. Camisasca, M. Rovere, P. Gallo, Mode coupling theory and fragile to strong transition in supercooled tip4p/2005 water, J. Chem. Phys. 144 (7) (2016) 074503, https://doi.org/10.1063/1.4941946.
[83] M. De Marzio, G. Camisasca, M. Rovere, P. Gallo, Microscopic origin of the fragile to strong crossover in supercooled water: the role of activated processes, J. Chem. Phys. 146 (8) (2017) 084502, https://doi.org/10.1063/1.4975387.
[84] M. De Marzio, G. Camisasca, M.M. Conde, M. Rovere, P. Gallo, Structural properties and fragile to strong transition in confined water, J. Chem. Phys. 146 (8) (2017) 084505, https://doi.org/10.1063/1.4975624.
[85] L. Xu, P. Kumar, S.V. Buldyrev, S.-H. Chen, P.H. Poole, F. Sciortino, H.E. Stanley, Relation between the widom line and the dynamic crossover in systems with a liquid–liquid phase transition, Proc. Natl. Acad. Sci. 102 (46) (2005) 16558–16562, https://doi.org/10.1073/pnas.0507870102.
[86] L. Liu, S.-H. Chen, A. Faraone, C.-W. Yen, C.-Y. Mou, Pressure dependence of fragile-to-strong transition and a possible second critical point in supercooled confined water, Phys. Rev. Lett. 95 (2005) 117802, https://doi.org/10.1103/PhysRevLett.95.117802.
[87] A. Faraone, L. Liu, C.-Y. Mou, C.-W. Yen, S.-H. Chen, Fragile-to-strong liquid transition in deeply supercooled confined water, J. Chem. Phys. 121 (22) (2004) 10843–10846, https://doi.org/10.1063/1.1832595.
[88] P. Gallo, M. Rovere, Mode coupling and fragile to strong transition in supercooled tip4p water, J. Chem. Phys. 137 (16) (2012) 164503, https://doi.org/10.1063/1.4759262.
[89] D. Corradini, P. Gallo, S.V. Buldyrev, H.E. Stanley, Fragile-to-strong crossover coupled to the liquid-liquid transition in hydrophobic solutions, Phys. Rev. E 85 (2012) 051503, https://doi.org/10.1103/PhysRevE.85.051503.
[90] P. Gallo, D. Corradini, M. Rovere, Fragile to strong crossover at the widom line in supercooled aqueous solutions of nacl, J. Chem. Phys. 139 (20) (2013) 204503, https://doi.org/10.1063/1.4832382.
[91] L. Lupi, P. Gallo, Mode coupling behavior and fragile to strong transition of trehalose in a binary mixture with water upon supercooling, J. Chem. Phys. 160 (24) (2024) 244501, https://doi.org/10.1063/5.0218369.
[92] J.R. Errington, P.G. Debenedetti, Relationship between structural order and the anomalies of liquid water, Nature 409 (2001) 318–321, https://doi.org/10.1038/35053024.
[93] J.M. Montes de Oca, F. Sciortino, G.A. Appignanesi, A structural indicator for water built upon potential energy considerations, J. Chem. Phys. 152 (24) (2020) 244503, https://doi.org/10.1063/5.0010895.
[94] N.A. Loubet, A.R. Verde, G.A. Appignanesi, A water structure indicator suitable for generic contexts: two-liquid behavior at hydration and nanoconfinement conditions and a molecular approach to hydrophobicity and wetting, J. Chem. Phys. 160 (14) (2024) 144502, https://doi.org/10.1063/5.0203989.